GAS-DYNAMIC LASER NOZZLE-UNIT AEROOPTICS

M. G. Ktalkherman and V. M. Mal'kov

UDC 533.697+532.517.4

1. Introduction. Aerooptics includes the phenomena associated with the passage of a laser beam through atmospheric inhomogeneities. One usually envisages the wave front distortions arising from passage through shock-wave structures, shearing and boundary layers, mixing layers, and wakes [1-3]. Such phenomena can occur when the laser is mounted on an aircraft [2]. Aerooptics differs from atmospheric optics in that the scale of the turbulent density pulsations is here less than the aperture size. Although the theoretical techniques in the two cases are in principle the same, the results are different [1, 4].

Phase aberrations do not occur merely when the beam passes in the external medium. In a fast-flow laser system, more importance attaches to the distortions that occur as the beam is formed in the cavity, since the phase-surface curvature in the near zone governs the intensity distribution in the far zone [5] and the deviations from the ideal case, where the radiation at the output would have a planar front.

Phase aberrations occur in the cavity in chemical and gas-dynamic lasers GDL on account of inhomogeneities in the flow beyond the nozzle array. The front curvature on passage through the medium governs the optical quality. We have examined the optical quality of the flow beyond planar nozzle arrays as commonly employed in GDL [6] and beyond honeycomb units [7] such as are used in chemical lasers and GDL. There is a second source of distortion in the laser itself, namely the aerodynamic windows, which separate the cavity from the external medium, which has been considered for example in [8].

Phase distortions occur at regular structures (shock-wave systems and contact surfaces) [9] and at turbulent ones (wakes and boundary and shearing layers). Turbulent scattering of light has been considered theoretically in [1, 10]. In experiment, the optical quality of a medium may be examined by interferometry or the focal-spot method [2]. In the first case, one obtains information on the phase distribution in the near zone, with the deviations from the mean averaged over the aperture, and where Strel's formula is used to calculate the far-zone intensity. In the second case, one obtains a direct result: one measures the intensity in the far zone. However, here as a rule one uses wide-aperture beams, i.e., averages over the entire aperture.

A certain spatial resolution is required to examine the effects on the optical quality of flow past nozzle arrays. The probe spot should of course be larger than these features in order that the averaging should be representative. It is clear that the averaged phase deviations may be less than the deviations determined on the full cavity aperture, since one does not consider for example the large distortions at the edges. However, if the changes in the averaged flow parameters in the cavity, in particular the density, are not sharp, the characteristic dimensions of such deviations are much greater than those of the probe spot, and the resulting relationships correctly reflect the phase changes associated with the internal turbulent structure. Of course, one does not consider the phase distortions associated with large-scale changes in the parameters (e.g., the optical wedge over the entire length), but this can in principle be done.

We used a relatively small-diameter beam to probe the flow in the cavity. The focal-spot method was used to examine how flow features beyond planar and honeycomb arrays affect the optical quality. If the optical results are to be interpreted correctly, it is necessary to have a detailed gas-dynamic picture for the flow. In [11-13], measurements were made on the averaged flow characteristics in a cavity for all the nozzle arrays used, while in [14] data were obtained on the turbulent-pulsation intensities for honeycomb units.

2. Apparatus. The measurements were made with a wind tunnel in which the nozzle arrays consisted of blocks of planar or honeycomb nozzles. The working part was 51 × 56 mm. Directly behind the nozzle array there were windows in all four walls of the working part. When the probe tests were done, the glass windows were replaced by inserts with holes for the sensors, which were displaced by micrometer screw devices.

Novosibirsk. Translated from Priklandaya Mekhanika i Tekhnicheskaya Fizika, No. 6, pp. 20-28, November-December, 1993. Original article submitted September 30, 1992.

0021-8944/93/3406-0761$12.50

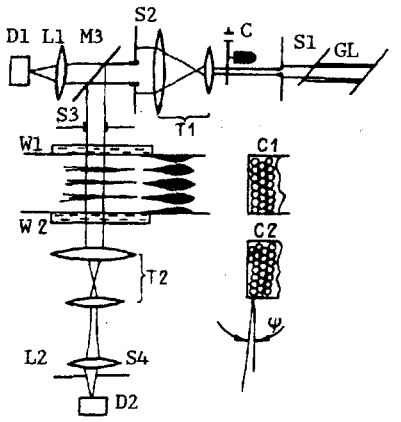

Fig. 1

The apparatus was flushed with dried air from cylinders. An ejector enabled us to operate in the stagnation pressure range p_0 = 0.6-4.0 MPa. A heater raised the inlet temperature to T_0 = 350 K. The Reynolds number is defined by the flow parameters in the exit section of the nozzle unit and the length of the nozzle and is $Re_L = (0.85\text{-}5.3)\cdot 10^6$, i.e., the flow conditions in the wakes were turbulent.

Nozzle Arrays. The planar nozzle arrays in each case were composed of three blades shaped on both sides and two side ones each shaped on one side. i.e., there were four planar nozzles, with the walls of the extreme ones in close contact with the walls of the working part as shown in Fig. 1. The shapes were identical in the supersonic parts of all the blades and were minimum-length contours defined by the characteristic method for Mach number M = 5 (adiabatic parameter k = 1.4) with correction for the boundary-layer displacement thickness. The size of the critical section was $h^* = 0.49$ mm, while the height of the section at the exit was H = 13.45 mm. The length of the supersonic part was L_c = 37 mm. The blade thickness t at the end where the convergence angle was $\alpha = 0$ varied: blocks I-IV had blades with t = 0.75, 0.5, 0.35, and 0.15 mm. Blocks III(1) and IV(1) were composed of the same blades as blocks III and IV but previously shortened by 7 and 11 mmcorrespondingly. Therefore, α in them was 2.5 and 4°, while t = 0.75 and 1 mm. The finite t and in them was 2.5 and 4°, while t = 0.75 and 1 mm. The finite t and α were required for strength but produced additional perturbations in the density patterns. Consequently, appropriate measurements were needed.

The honeycomb nozzle was an array of compactly placed conical micronozzles. We used arrays with the following characteristics for the optical measurements: expansion angle of an individual micronozzle 20°, diameter of critical section 1 mm, degree of expansion 25. The ratio of the working-channel area to the total critical-section area was as in the planar arrays (about 29). It is important to keep this parameter constant because it governs the mean density level. We tested two such nozzles: in unit Cl, the range of micronozzles was parallel to the optic axis, while in C2, they were at 13° (Fig. 1).

Measurements. The gas-dynamic structures were examined by schlieren and probe methods. Schlieren photographs were taken with various positions of the knife-edge by means of a spark source giving a pulse length of about 1 μsec. The total and static pressure patterns were measured with Pitot tubes having receiving parts 0.25 × 1 mm and a static pressure fitting with a rounded tip of diameter 1 mm. The other flow parameters were derived on the assumption of constant stagnation temperature: the velocity and density. The measurements were made at several sections in the channel at 170 mm from the end of the nozzle. The methods have been given [14] for examining the pulsation characteristics of flows from honeycomb arrays.

Figure 1 shows the essential scheme for measuring the optical characteristics, which was analogous to that in [15]. The beam from the laser GL ($\lambda = 0.63$ μm) passed through the chopper C and the telescopic system Tl, which expanded it to a diameter of about 30 mm. Then the stop S2 selected the part with the most uniform intensity of diameter about 9 mm. The semitransparent mirror M3 split the beam into two: one beam was directed to the reference detector D1 and the other went through the object. This beam after passage through the windows Wl and W2 and the second telescopic system T2 (reversed) was focused, i.e., the beam diameter was reduced, which enabled us to realize the far zone at short distances. Lens L2 collected the radiation on the receiving area of the detector D2. The signal was measured with a differential system, i.e., we measured the difference in the signals between D1 and D2. For the experiment, the signals at the detectors had been equalized with a loading device that set the zero. When the beam passed through the inhomogeities, a difference signal ΔI arose, which was recorded by a differential oscilloscope. The total signal I_0 was measured before and after the experiment. The result was taken as correct when I_0 was the same before and after the experiment, while the differential signal returned to zero.

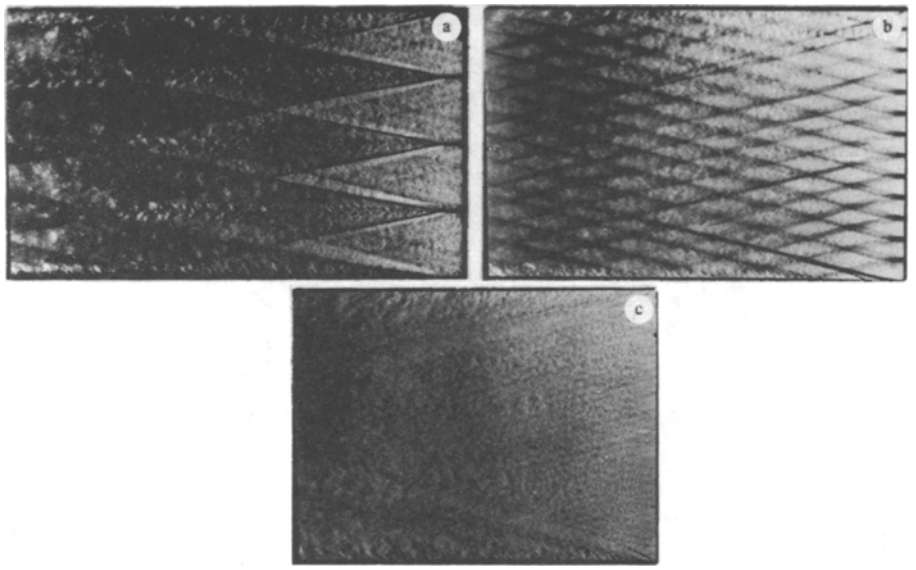

Fig. 2

The system was very sensitive to the position of the glass parts. During start-up, when a shock wave passes, minor displacements may occur. Therefore, we used the results only from those cases where there was no change on start-up in the zero signal or in the total ones. Also, each experimental point was measured several times.

There is also a possible effect from the over-all displacement of the beam at the inhomogeneities, which would produce a fictitious reduction in the probe radius and intensity. In [15], measurements were made on the optical quality of circular supersonic jet, where the effect was observed, and the displacement was balanced out during the experiment by means of a plane-parallel plate placed after the reversed telescope. In our case, deviation of the beam from the detector did not occur because the object was of plane-parallel type and the flow pattern in the chamber was strictly symmetrical. However, a check was made for it before and during the experiment, for which in particular we used stop S4. This was inserted on the first dark ring beyond the Airy disk (stops S1 and S2 served to eliminate surplus fringes).

3. Experimental Results, Discussion, Aerodynamic Measurements. Figure 2 shows schlieren photographs of the flow behind the arrays with the knife-edge in the vertical position: a) planar array with t = 0. 5 mm, b) honeycomb array Cl, and c) honeycomb C2. The blade ends are visible in Fig. 2a. The flow around the ends was accompanied by expansion in the bottom part with subsequent rotation of the flow in the shock waves. The light regions are the fans of expansion waves and the dark lines are the density-increase steps. A characteristic feature is the rhomboid structure in these steps, with a negative-pressure wave gradually dying away downstream. The boundary layer flowing from the nozzle walls formed a distinct wake beyond the blade edges. It had a reasonably periodic vortex structure, with the dimensions of the vortices increasing away from the end. There were no perturbations at the core of the flow at the exit, which shows that the nozzle contour is of good quality. So far as one can judge from the photographs, the density-increase steps and negative waves from adjacent blades do not cause any visible change in the wake width and structure.

Similar flow patterns have previously been examined in connection with the bottom resistance for various bodies. One of the marked differences in the conditions in our experiment was that the height of the boundary layer δ at the end was several times greater than the thickness t of the edge of the nozzle. Experiments in which the ends of the blades were drained show that the bottom pressure substantially exceeds the corresponding value obtained with $\delta/t \to 0$, the values characteristic of other technical applications. For example, for the array with t = 0.75 mm (at p_0 = 0.7 MPa), the pressure at a blade edge was only half the pressure at the end of the nozzle.

Another difference in the wake under our conditions was that the parameters were variable (usually considered as constant) in the flow external in relation to the wake, i.e., in the core of the jet from an individual nozzle. Figure 3 shows for example $\bar{\rho}_{0E}$ (x) and $\bar{P}_{0E}(x)$, the ratios of the densities and pressures at the axis in the core of the flow to the corresponding values in the forechamber, with x the distance from the end of the array. The differences in thickness and angle of inclination at the ends of the blades did not affect the axial distributions $\bar{\rho}_{0E}(x)$ and $\bar{P}_{0E}(x)$, while the changes in those parameters along the flow were small (the Mach numbers at the cores also varied, with only M(x) decreasing). There was considerable nonuniformity in the density profiles in cross section, and the larger t, the greater the deviations $\Delta\rho$ from the mean value

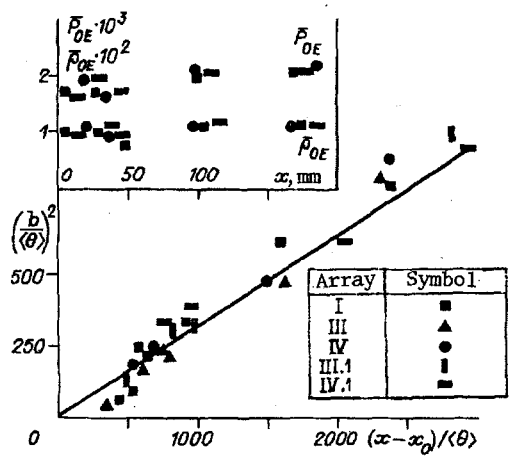

Fig. 3

$<\rho>$. With array I, for example, $\Delta\rho/<\rho> = \pm 12\%$ at the start of the cavity. The nonuniformities were smoothed out downstream, and $\Delta\rho/<\rho> \sim \pm 5\%$ at x = 160 mm.

The distribution of the dimensionless density deficiency along the wake axis was described by means of self-similar variables for the distant wake. The dependence

$$\left(\frac{\rho_E}{\rho_E - \rho_0}\right)^2 = f\left(\frac{x}{\langle\theta\rangle}\right)$$

was the same in all the models and agreed with the data for an incompressible isobaric wake (ρ_0 and ρ_E are the density at the axis and the boundary of the wake correspondingly, while $<\theta>$ is the mean momentum-loss thickness taken along the flow). The density-deficiency profile in the cross section of the wake took the usual form (Gaussian function) and was the same for all the planar arrays, although the spread in the points was much larger than that in the velocity-deficiency profile.

The wake half-width b(x) was determined from the coordinates, where $(u_E - u)/(u_E - u_0) = 0.5$ (u is the flow speed, while the subscripts E and 0 as before correspond to the conditions at the external boundary of the wake and at the axis). Figure 3 shows b(x) in self-similar coordinates, where x_0 is the effective start of the wake. We show the data for all t and α. There is a satisfactory correlation between the data for the different t and α. Here b(x) is almost as in the case of an incompressible isobaric wake (straight line) with a new value for x_0 as determined in the experiments (x_0 is dependent on the wake generator shape).

This gave all the data for semiempirical flow calculation in the cavity, including the averaged wake characteristics. The main interest attached to the density pattern and the wake width, so only these results are given, and those only partially. The gas dynamics of planar arrays have been described in detail in [11].

Honeycomb-nozzle gas dynamics may be found in [7, 12-14]. Studies have been made on the effects of array geometry and individual micronozzle shape on the downstream decay in the density inhomogeneities. At $\bar{X}_d = x/d_e \approx 10$ (d_e is the exit-section diameter of a micronozzle), $\Delta\rho/<\rho> = 20\text{-}15\%$, and the required inhomogeneity level of 1% is attained at $\bar{X}_d \approx 70\text{-}100$. The pulsations in the mass flow rate are $<m> = 6\text{-}4\%$ (in accordance with the array geometry) in the $\bar{X}_d = 10$ section, while at $\bar{X}_d = 20\text{-}30$ the quantity is further halved and subsequently falls very slowly and slightly along the channel.

Aerooptic Measurements. The normalized intensity (Strel intensity) is the ratio of the maximum intensity I at the center of the beam after the perturbed medium to the intensity I_0 that would occur in the absence of aberrations, and at small aberrations it is proportional to the mean-square wave front deformation and is independent of the type of aberration [5]:

$$I/I_0 \approx 1 - (2\pi/\lambda)^2 (\Delta\varphi)^2, \quad \text{or} \quad \Delta I/I_0 = \overline{\Delta I} \sim (\Delta\varphi)^2 \quad (\Delta I = I - I_0).$$

The wave equation has been integrated [4] for propagation in a turbulent medium (Gaussian and actual autocorrelation functions for the turbulence were considered), and it was shown that the phase change is

$$\Delta\varphi = \frac{2\pi}{\lambda}\beta\sqrt{\Lambda L}\,\frac{\Delta\rho'}{\rho}\left[\frac{\rho}{\rho_0}\right], \tag{3.1}$$

in which Λ is the turbulence scale, L the scattering layer thickness, β the Gladstone–Dale constant, λ wavelength, ρ density, $\Delta\rho'$ density pulsation, and ρ_0 density under normal conditions.

Shock waves and wakes are the main perturbing factors in a supersonic flow beyond a planar array, and there is much experimental evidence on the structures and characteristics in turbulent wakes and layers, and the following evaluations can

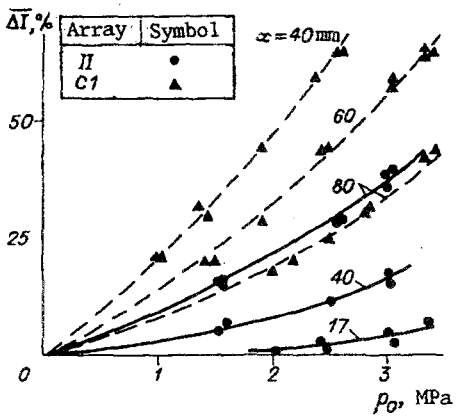

Fig. 4

be made. The turbulent scale is proportional to the layer thickness: for shearing layers and mixing ones [16] $\Lambda = 0.25L$, while it is found [17] for boundary layers that an acceptable approximation is $\Lambda = 0.1L$. Measurements on the wake behind a flat body [18] gave $\Lambda = 0.5L$. Then always $\Lambda \sim L$. The increase in wake thickness L in our case (Fig. 2) is closely approximated by $\sqrt{x}$, while $\Delta\rho/\rho$ in the wake varies [18] only over an initial short section, subsequently remaining almost constant. Then the general behavior of $\overline{\Delta I}$ should be determined by two terms:

$$\overline{\Delta I} \sim x\rho^2. \tag{3.2}$$

Figures 4 and 5 show that $\overline{\Delta I}$ measurements for planar arrays agree well with (3.2). Figure 4 shows the p_0 dependence of $\overline{\Delta I}$, while Fig. 5 shows the dependence on distance x at the points where the measurements were made (in all cases, the origin for x was taken at the end of the supersonic part of the blade, including for arrays with shortened blades). The pressure dependence is close to quadratic, while the x dependence is linear, so in the main the scattering occurs here at turbulent wakes. If the intensity of the shock-wave structure were the decisive factor, $\overline{\Delta I}$ should decrease downstream.

This increase in $\overline{\Delta I}$ with x is similar to a certain extent to that of an optical wedge, whose presence has been observed previously, but which was ascribed to density increase in the channel. These results show that the increase in $\overline{\Delta I}$ in our case cannot be explained simply by a density gradient: the increase in ρ over 100 mm is only 10-15% (Fig. 3), while the proportion of scattered radiation is doubled or more at 50 mm in accordance with the pressure level. This is important, since an optical wedge could be eliminated by appropriate cavity adjustment if that wedge were associated only with the density gradient down the flow. The data show that phase changes beyond planar arrays cannot be balanced out by adjustment, since they are due to the turbulent wake (increase in the turbulence scale Λ).

An unexpected point is that the results for all the planar arrays are almost the same. Figure 5 gives points for $p_0 = 2.4$ MPa for three arrays having various t and α. All the points lie on a single straight line, so Figs. 4 and 5 show data only for certain arrays. Aerodynamic measurements show (Fig. 3) that the wake thicknesses are identical in our case, but one anticipates that there may be changes in the turbulent characteristics, particularly for the shortened arrays, when the angle of convergence at the end of a blade is appreciable. At the same time, the shock-wave intensities beyond the array increase with t and α. The identical $\overline{\Delta I}$ indicate firstly that the effects from the shock-wave structure are sight and secondly that not only are the averaged wake characteristics identical (for the given geometry) but also the turbulent ones are similar (scale and pulsation intensity).

Figure 4 gives some scattering results for honeycomb arrays (the p_0 dependence of $\overline{\Delta I}$ is analogous to that for planar arrays). Figure 6 shows the behavior of $\overline{\Delta I}$ along the cavity for C1 and C2 arrays. It has been suggested [19] that the optical quality is dependent on the cavity orientation. Parts b and c of Fig. 2 give a qualitative indication of how the visible homogeneity improves when the optic axis of the cavity is rotated. Figure 6 shows that there is a marked improvement in quality in the initial part because the honeycomb arrays have strictly ordered nozzle packing in the rows, while the different optical paths along the cavity axis placed along the nozzle rows differ considerably, e.g., for a ray passing along the axis of the nozzles and for a ray passing along the parts separating the individual nozzle rows, since in the second case the ray is always in the wake region. A certain degree of chaos is produced by directing the optic axis at an angle ψ to the lines of nozzle rows, which tends to equalize the optical paths. Of course, there are optimal ψ.

Calculations have been performed [19] on the geometry of the shock waves emerging from nozzle edges (the discussion concerned the two-dimensional case (planar arrays) and the three-dimensional one (honeycomb arrays)), and a nonviscous

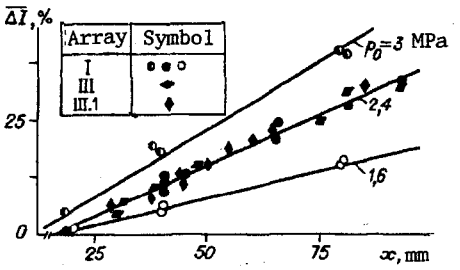

Fig. 5

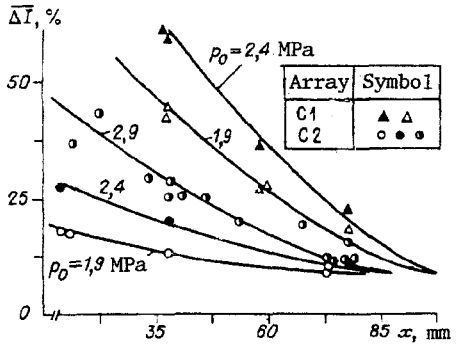

Fig. 6

formulation was used to determine the parameter changes at the these steps and the density differences $\Delta\rho$. When the $\Delta\rho$ had been determined, the optical paths were calculated for various ψ. The main perturbing factor in the initial part of the flow is the jet geometry, and the result for ψ (but only for ψ) will coincide with that from exact calculations and experiments. However, that formulation is essentially incorrect. Firstly, the flow around the edges gives rise not only to density-increase steps but also to negative-pressure ones (light regions in Fig. 2a), and secondly, the main scattering mechanism for planar arrays and honeycomb ones is that at turbulent wakes. The nonviscous model cannot in principle explain the behavior of $\overline{\Delta I}$ for example as a function of x. Figures 5 and 6 show that the behavior of $\overline{\Delta I}$ for a planar array is opposite in character to that for a honeycomb one, although in both cases the averaged-density gradient is positive, while the intensity of the shock-wave structure falls downstream.

A free turbulent layer develops and expands and extends to new parts of the flow, as for the wakes beyond blades, and Λ increases. Figure 2a shows this clearly. The wakes from the edges of each nozzle merge quite rapidly with the honeycomb arrays because of the small characteristic dimensions, and one gets a flow uniform over the entire channel, and which has a smaller Λ than would be the case for planar arrays. Figure 6 shows that the initial difference in the $\overline{\Delta I}$ for arrays C1 and C2 is controlled by the jet geometry but is lost over a distance of 80 mm (or 15 times the exit section d_e of an individual nozzle), i.e., the flow becomes homogeneous from the optical viewpoint. Further downstream, the $\overline{\Delta I}$ for the two arrays will evidently coincide. The point where the difference between the flow patterns for C1 and C2 vanishes from the optical viewpoint will vary clearly with d_e, i.e., the smaller d_e, the closer that point to the origin.

The fall in $\overline{\Delta I}$ along the cavity is due to the intensity reduction in the turbulent pulsations beyond a honeycomb array [14]. That intensity in the mass flow rate $<m>$ falls by a factor two over about 30 times the diameter, and subsequently the intensity falls slightly along x. The behavior of $\Delta\rho'$ is analogous to that of $<m>$. If the reduction in $\overline{\Delta I}$ were due to the reduction in the averaged-density differences $\overline{\Delta\rho}$, then $\overline{\Delta I}(x)$ would have its least values at 70-100 times the diameter. In fact, $\overline{\Delta\rho}(x)$ behaved in that way in the [7, 12, 13] measurements.

Figures 5 and 6 thus imply that planar arrays give no advantages over honeycomb ones for cavities having size along the flow of about 80 mm (and the more so for larger ones). Also, the angle $\psi = 13°$ was not optimal in our experiments. Calculations [19] give the first minimum for $\overline{\Delta I}$ at $\psi = 15°$.

From (3.1) one can convert the model-experiment results to real laser conditions. Transfer to other λ does not alter the situation qualitatively, since one of the basic parameters characterizing the solution is the ratio of the aperture to the turbulence scale [4]. Incorporating a large number of wakes has been considered in [20]. The wake dimensions and turbulence scale have been estimated from the actual Reynolds numbers.

The main result is that joint examination of the aerodynamic and aerooptic characteristics for nozzle arrays in gas-dynamic and chemical lasers demonstrates that scattering under these conditions occurs at turbulent wakes, and the main trends in the phase change in a beam passing through such a medium can be explained by the wake structure and dimensions.

We are indebted to V. P. Malyavin and V. A. Feofilaktov for initiating this study and to N. A. Ruban and G. V. Klimchik for assistance in performing the experiments and formulating the results.

REFERENCES

1. G. W. Sutton, "Aero-optical foundations and applications," AIAA J., **23**, No. 10 (1985).
2. Progress in Astronautics and Aeronautics: Aero-Optical Phenomena, Vol. 80, edited by K. Gilbert and L. Otten, AIAA, New York (1982).
3. A. E. Fuhs, "Overview of aero-optical phenomena," Wavefront Distortions in Power Optics, Vol. 293, A. Fuhs and S. Fuhs (eds.), SPIE, Washington (1981).
4. G. W. Sutton, "Effect of turbulent fluctuations in an optically active fluid medium," AIAA J., **7**, No. 9 (1969).
5. M. Born and E. Wolf, The Principles of Optics [Russian translation], Nauka, Moscow (1973).
6. S. A. Losev, Gas-Dynamic Lasers [in Russian], Nauka, Moscow (1977).
7. D. A. Russel, S. E. Neice, and P. H. Rose, "Screen nozzles for gas-dynamic lasers," AIAA J., **13**, No. 5 (1975).
8. E. M. Parmentier and R. A. Greenberg, "Supersonic flow aerodynamics windows for high-power lasers," AIAA J., **11**, No. 7 (1973).
9. H. W. Liepmann and A. Roshko, Elements of Gasdynamics, Wiley, New York (1957).
10. C. J. Knight, G. W. Sutton, and R. Berggren, "Phase aberrations and laser output beam quality," Wavefront Distortions in Power Optics, Vol. 293, A. Fuhs and S. Fuhs (eds.), SPIE, Washington (1981).
11. M. G. Ktalkherman, V. M. Mal'kov, and N. A. Ruban, "Flow characteristics from planar supersonic nozzlew arrays," Report 2090, ITPM AN SSSR, Sib. Otd. (1991).
12. M. A. Anikin, M. G. Ktalkherman, V. M. Mal'kov, and A. P. Sinitsyn, "Dependence of flow parameters beyond a hoenycomb array on the individual micronozzle expansion angle," in: Gas Dynamics of Gas-Dynamic Laser Flow Parts: Coll. in Russian ITPM, Sib. Otd. AN SSSR (1987).
13. V. K. Baev, M. G. Ktalkherman, V. M. Mal'kov, and N. A. Ruban, "Flow characteristics and pressure recovery in a rectangular channel beyond an array of axisymmetric nozzles," in: Gas Dynamics of Flows in Nozzles and Diffusors: Coll. [in Russian], ITPM, Sib. Otd. AN SSSR (1982).
14. V. N. Zinov'ev, M. G. Ktalkherman, V. A. Lebiga, and V. M. Mal'kov, "Averaged and pulsation characteristics of a supersonic flow in a wind tunnel containing a honeycomb nozzle," Izv. SO AN SSSR, Ser. Tekhn. Nauk, No. 5 (1989).
15. D. W. Bogdanoff, "Optical quality of supersonic jets of various gases," Appl. Optics, **21**, No. 5 (1982).
16. R. G. Butt, "Turbulent mixing of passive and chemically reacting species in a low-speed shear layer," J. Fluid Mech., **82**, 53 (1977).
17. G. W. Sutton, "Optical imaging through aircraft turbulent boundary layers," Progress in Astronautics and Aeronautics: Aero-Optical Phenomena, Vol. 80, edited by K. Gilbert and L. Otten, AIAA, New York (1982).
18. A. Demetriades, "Observation on the transition process of two-dimensional sueprsonic wakes," AIAA J., **9**, No. 11 (1971).
19. T. S. Vaidyanathan and D. A. Russel, "Wave-generated disturbance downstream of a nozzle array," AIAA J., **23**, No. 5 (1985).
20. D. W. Bogdanoff, "The optical quality of shear layers: prediction and improvement thereof," AIAA J., **22**, No. 1 (1984).1